D5

N79-20035

5

APPLICATION OF DIRECT-INVERSE TECHNIQUES TO AIRFOIL ANALYSIS AND DESIGN*

Leland A. Carlson
Bruce M. Rocholl**
Texas A&M University

SUMMARY

During the past few years, the direct-inverse technique has been developed into a numerical method, called TRANDES, that is suitable for the analysis and design of subsonic and transonic airfoils and for the evaluation of design concepts. This paper provides a general description of the method, demonstrates its application to a design-analysis type of problem, and finally, discusses a new usage of the method for the low speed high lift case.

INTRODUCTION

The basic concept of the present method (refs. 1-4) is to have a technique which can be used in either the direct (analysis) mode in which the airfoil shape is prescribed and the flowfield and surface pressures are determined, or in the direct-inverse (design) mode in which an initial nose shape is given along with the pressure distribution on the remainder of the airfoil. In the latter case, the flowfield and actual airfoil shape are computed.

The resultant computer program, called TRANDES, (ref. 5), has several unique features. In order to achieve accuracy, the method utilizes the full inviscid potential flow equation; and in order to remain simple, it solves the problem in a stretched Cartesian grid system that maps the infinite physical plane to a rectangular computational box. Further, to avoid at supersonic points difficulties associated with nonalignment of the coordinates and the flowfield, a rotated finite difference scheme is used in the solution; and the resulting transformed finite difference equations are solved iteratively by column relaxation sweeping from upstream to downstream. Finally, the method does include the effects of weak viscous interaction. The basic idea in the design case is to treat the airfoil determined by the inverse method as the displacement surface and to subtract from it a displacement thickness determined by a Nash-Macdonald (ref. 6) turbulent boundary layer computation in order to obtain the actual airfoil coordinates. It should be noted that the present program determines the airfoil shape simultaneously

*Supported by NASA Grant NSG 1174
**Presently with the Boeing Co., Seattle, WA

with the flowfield relaxation solution. For the analysis case, the approach is to calculate a boundary layer displacement thickness and to use it to correct the location of the displacement surface (i.e. airfoil ordinate plus δ^*). The flowfield is then solved iteratively with the displacement surface being updated every ten relaxation cycles.

Now, in the design mode, the shape of the nose region (typically 6-10% chord) is specified and a pressure distribution is prescribed over the remainder of the airfoil. Thus, the appropriate airfoil boundary condition in the direct region near the leading edge is the surface tangency requirement and in the inverse region, where the pressure is specified, it is essentially the specification of the derivative of the perturbation potential in the x-direction. In order to satisfy these at the airfoil boundary, which in general will not coincide with the Cartesian grid points, the derivatives in the boundary conditions are expanded as two term Taylor series about a dummy point inside the airfoil. The derivatives in these series are then written in finite difference form using second order formulas for all first derivatives and at least first order ones for higher derivatives. In the direct region, central differences are used for x-derivatives and forward (on the upper surface) for the y-derivatives. However, to prevent numerical instability, the inverse region uses a second order backward difference formula for the first term of the Taylor series representing the x-derivative. For details concerning the finite difference formulation, boundary conditions, etc., see references 2-5, and 7.

Currently, the program can be easily used to design or analyze an airfoil at a specific flight condition. Figure 1 shows such a result for the design of a low lift airfoil having a sonic rooftop followed by a linear recovery. Supercritical shockless airfoils have also been designed and examples are presented in reference 7.

Now any numerical method needs to have its accuracy verified. As a result, comparisons with other methods (refs. 8,9) have been conducted for airfoils ranging from 4 to 16% thick and Mach numbers up to 0.85. Some of these results are presented in references 2, 4, and 10; and, in general, the agreement is excellent. In addition, comparisons have been made with transonic experimental data obtained at the NAE (Ottawa) (ref. 7) and at the Ohio State University. A typical comparison with the OSU data is shown for the GA(W)-2 airfoil in figure 2. In general, the agreement for C_P, C_L, C_D, and C_M is quite acceptable.

Symbol definitions are given in an appendix.

APPLICATION TO DESIGN

To demonstrate the usefulness of the present combined design-analysis method, consider the problem of designing an airfoil having a rooftop plateau followed by a Stratford recovery (ref. 11). (It should be noted that a Stratford recovery is used here only for example purposes. While such a pressure distribution has the advantage that it maintains the boundary layer at a constant margin from separation, it also has several disadvantages which will

be mentioned later). In addition, two design concepts will be compared. In the first case, the airfoil will be designed at a low C_L with a sonic upper surface rooftop pressure plateau; while in the second case, the airfoil will be designed with a supercritical plateau at a moderate C_L. The airfoils will then be analyzed and compared at conditions other than the design point to see which one has the better characteristics.

The results for the critical rooftop design, which had a target C_L of 0.35, are shown in figure 3. The solid line is the design C_P distribution, and the final airfoil shape after accounting for the boundary layer is the one shown. Notice the reverse curvature on the upper surface and the resultant airfoil thinning. This behavior is typical of airfoils employing Stratford distributions, and frequently it leads to shapes that are structurally too thin in the vicinity of the trailing edge.

How was this shape obtained? Since the method requires the specification of the leading edge region, the nose shape can be used to control the trailing edge thickness. This approach is demonstrated in figure 4 and works easiest if an analytical nose shape controlled by a single parameter is utilized. Here the nose shapes are those associated with NACA 00XX airfoils. Notice that as the shape parameter increases, the trailing edge thickens. In addition, it should be noted that all the results in figure 4 were obtained using the same C_P boundary conditions and that each case is completely independent. Thus, obvious physical unrealities such as trailing edge crossing do not affect the final design shape. Also, asymmetric nose shapes may be used.

As indicated by figure 4 and shown specifically in figure 5, there is a unique relationship between the values of the nose shape parameters and the trailing edge ordinates. Usually the variation is essentially linear; and thus, after obtaining the results for two cases, the desired trailing edge ordinates can be obtained on the third try.

Sometimes in an aft-camber design case if the computed upper and lower surfaces are not almost parallel near the trailing edge, the flow in that vicinity will deviate from the desired pressure distribution and try to stagnate, with resultant separation. Usually by slightly adjusting back and forth the starting point of the upper surface recovery, a location can be found which will yield acceptable trailing edge slopes and pressures. This procedure may require a few extra iterations and some adjustment in nose shape, but it is normally not difficult.

Figure 6 shows the design pressure distribution and resultant airfoil shape obtained when the airfoil was designed for a higher C_L and with a Mach 1.1 supercritical rooftop. Since this airfoil was designed at higher lift (C_L = .55), the lower surface pressure distribution had a larger aft bucket. This case demonstrates the disadvantage of using a Stratford recovery on a highly aft-cambered airfoil in that the airfoil thickness is less than 2% aft of 80% chord.

Now an essential requirement of a design method, from an engineering

standpoint, is that when the designed airfoil is analyzed at the design condition, the computed C_p distribution should agree with the C_p distribution used for the design. Such analysis results are shown in figures 1, 3, and 6 and were obtained using the present method with viscous interaction included. As can be seen, the agreement is excellent. It is believed that these comparisons verify the engineering consistency of the method and, since the analysis results usually agree with experimental data, that the airfoils designed by this method should perform as predicted.

APPLICATION TO ANALYSIS

One of the difficulties associated with using a Cartesian grid for an analysis computation is that such a grid does not place a large number of points near the leading edge. Thus, the wave drag coefficient, which is determined by integration of the pressure coefficient, has an inherent error. Previous studies have determined this error is consistent and primarily a function of airfoil shape and grid spacing; and thus, correction factors can be determined from calculations at subcritical speeds where the wave drag should be zero. Unfortunately, the correction procedure suggested in reference 5 may be partially in error; and while research is continuing, the results presented in this section have been obtained using the following technique.

At a Mach number, $M_{\infty_{sub}}$, for which the flow is entirely subcritical, determine for each angle of attack, α, the normal, $C_{N_{sub,\alpha}}$, and axial, $C_{A_{sub,\alpha}}$, force coefficients. Then find the drag correction from

$$\Delta C_{DW_{sub,\alpha}} = C_{A_{sub,\alpha}} + C_{N_{sub,\alpha}} \tan\alpha$$

Next find the correction at the desired supercritical Mach number, M_∞, by

$$\Delta C_{DW_{M_\infty,\alpha}} = \Delta C_{DW_{sub,\alpha}} \sqrt{\frac{1-M_{\infty_{sub}}^2}{1-M_\infty^2}}$$

Then correct C_A at M_∞ by

$$C_{A_{corr}} = C_{A_{orig}} - \Delta C_{DW_{M_\infty,\alpha}}$$

and find

$$C_{DW_{M_\infty,\alpha}} = C_{N_{M_\infty,\alpha}} \sin\alpha + C_{A_{corr}} \cos\alpha$$

The total drag is then given by

$$C_D = C_{DW} + C_{DF}$$

where C_{DF} is the skin friction drag determined by the Squire-Young method. While not perfect, this approach seems to yield good estimates. Also, the investigation is continuing and the method does not as yet include a correction for non-conservative differencing. Finally, $M_{\infty_{sub}}$ used to determine the correction factors should be as high as possible.

Some typical analysis results are shown in figures 7-9. Figure 7 shows the effect of varying angle of attack at the design Mach number for Airfoil 109B (critical rooftop design), while figure 8 portrays variations due to changes in M_∞. As α increases, the flow on the upper surface goes supercritical and a shock forms. However, there is a desirable pressure plateau aft of the shock wave (ref. 12) which will permit boundary layer recovery. While the analysis results indicate no separation for the conditions shown, there probably would be shock induced separation at higher α's. Because of the Stratford recovery, such separation would probably lead to a large separated region and a very sharp break in the C_L (α) curve.

As can be seen in figure 8, as M_∞ increases a supersonic bubble forms and grows and eventually terminates in a shock wave for $M_\infty \geq 0.79$. Aft of the supersonic zone, the pressures closely follow the original design distribution with no separation. These, and other studies, showed that at a C_L of 0.35, drag divergence occurs at M_∞ of 0.78.

Similar studies were performed for Airfoil 209 (supercritical rooftop design), and the angle of attack variation is shown in figure 9. Note that the pressure distribution variation at positive angles of attack is considerably different from that of Airfoil 109B (fig. 7) in that a shock wave forms immediately and C_D increases rapidly. Interestingly, the upper surface pressure continues to follow the original Stratford recovery aft of the shock wave. Also, other studies indicate possible shock induced separation for $M_\infty \geq 0.77$ even at zero angle of attack.

Analysis results such as these can also be used to compare airfoils obtained using different design philosophies. An example for the two designs being considered here is shown in figure 10. Notice that for Airfoil 109B, C_D is relatively constant up to C_L's of 0.55, while Airfoil 209 exhibits a steady increase in C_D. In addition, other calculations indicate that 109B has little or no drag creep for $0.5 \leq M_\infty \leq 0.74$ and $C_L \leq 0.5$. However, Airfoil 209 has 6-18 counts of drag creep in the same range.

Now it should be pointed out that these results <u>are not</u> critical of supercritical airfoils. In fact, Airfoil 109B, whose shape was determined by the inverse method using a "critical" rooftop could be used at C_L's up to 0.55 with low drags. Thus, it is in essence a supercritical airfoil and could be used at design lift coefficients up to 0.55. The point is that with the design philosophy and assumptions used in these examples, the inverse technique appears to yield the best results by designing the shape with a critical rooftop at a low C_L. The airfoil then can, at least in this case,

be used at higher lift coefficients.

APPLICATION TO THE HIGH LIFT CASE

A few years ago Barnwell (ref. 13) demonstrated that the direct-inverse technique could be successfully applied to the low speed high lift case. By specifying the separation point, he was able to obtain excellent agreement with experiment by solving the small perturbation equation with direct boundary conditions upstream of separation and inverse boundary conditions (pressure specified) downstream of separation. Thus, the question arose -- could similar results be obtained using the full potential flow equation with viscous interaction and letting the separation point be determined as part of the solution?

With these ideas, the low speed high lift case has been modeled as shown in figure 11; and TRANDES has been appropriately modified. On the lower surface, the flowfield is determined using direct boundary conditions (airfoil specified) including the effects of weak viscous interaction. On the upper surface, the flowfield is also computed directly, with viscous interaction up to the separation point, which is determined as part of the solution. Downstream of separation, inverse boundary conditions are utilized; and the pressure is assumed to be constant in the separated zone. The present studies have shown that the separated zone pressure, which is computed as part of the solution, must be determined by conditions at both the separation point and at the trailing edge and not just on conditions in the vicinity of separation. This result is in agreement with the conclusion of Gross (ref. 14) that conditions at the downstream end of the separation bubble determine bubble pressure. For the present studies, it has been found adequate to approximate the separated pressure by

$$C_{P_{sep}} = \frac{-2(\phi_{ITE} - \phi_{sep})}{\Delta x}$$

where ϕ_{ITE} and ϕ_{sep} are the perturbation potentials at the trailing edge and the separation point, respectively.

Now in principle, the separated wake region should probably be accurately modeled with respect to physical phenomena and details; and this approach has been taken by other investigators (refs. 14-17). In the present model, however, the wake is treated very simply in that it is assumed to be inviscid with a constant pressure across the pseudo trailing edge formed by the upper and lower displacement surfaces.

Finally, initial calculations with this model have indicated that the separation point location, and thus the lift, is strongly dependent upon the boundary layer transition point. Thus, the viscous interaction scheme in TRANDES has been modified to include an initial laminar boundary layer (computed by a compressible Thwaites method), natural transition, and then a

turbulent boundary layer computed by the Nash-Macdonald method. For those cases where laminar separation occurs prior to separation, a long or short bubble, depending upon local flow conditions, is empirically modeled, and then transition is assumed.

The calculation procedure uses the same iterative successive column relaxation scheme used in the basic program except that the separation point and separated pressure level are permitted to vary. A convergence history for a typical case is shown in figure 12. Initially some oscillation occurs on each grid; but, as can be seen, the values quickly converge. Normally, four hundred iterative cycles are performed on both the medium and fine grids. The former normally yields 66 points on the airfoil, while the latter yields 130.

Results for a GA(W)-2 airfoil are shown in figures 13 and 14. In both cases, the lower surface remained entirely laminar, although results with an all turbulent lower surface boundary layer showed no significant differences. On the upper surface transition with a short separation bubble occurred near the leading edge. In general, comparison with experimental data (ref. 18) is good with respect to C_p, separation point, separated pressure level, and C_L; and thus the method is quite promising.

Figure 15 shows a comparison with experiment of C_L versus angle of attack for the same airfoil. Similar results have also been obtained at other Reynolds numbers. At the present time, research on this approach to the high lift problem is continuing in order to ensure that $C_{L_{max}}$ can be determined accurately.

As a final note, this procedure has also been applied to Airfoil 109B discussed previously. Surprisingly, the design Stratford recovery used at Mach 0.74 seems to also affect the low speed flow since a sharp break occurred in C_L (α) at 19 degrees and a C_L of 2.08, indicating another disadvantage of using a Stratford recovery.

CONCLUDING REMARKS

Based upon the results presented here, the following remarks can be stated: (1) The present viscous analysis method (TRANDES) is suitable for engineering estimates of transonic airfoil data; (2) The present inverse design method accounts for the effects of weak viscous interaction in the airfoil design process and is numerically consistent with analysis results; (3) The complete potential flow equation coupled with a boundary layer method can be used in a direct-inverse fashion to accurately compute the flow about airfoils at low speeds having massive separation.

APPENDIX

SYMBOLS

C_A	axial force coefficient
C_D	two-dimensional drag coefficient
C_{DF}	profile drag coefficient
C_{DW}	wave drag coefficient
C_L	two-dimensional lift coefficient
C_M	two-dimensional quarter chord moment coefficient
C_N	normal force coefficient
C_P	pressure coefficient
c	chord
M_∞	freestream Mach number
RN	freestream Reynolds number
α	angle of attack
ΔC_{DW}	wave drag coefficient correction
δ^*	boundary layer displacement thickness
δ_{te}	trailing edge thickness
Δx	length of separated region
ϕ	perturbation potential

Subscripts

corr	corrected value
ITE	trailing edge
sep	separation point or region
sub,α	case where flow is entirely subcritical and at angle of attack α
orig	uncorrected original value
M_∞,α	at angle of attack α and Mach number M_∞

REFERENCES

1. Carlson, L.A.: Inverse Transonic Flow Calculations using Experimental Pressure Distributions. AIAA Journal, Vol. 12, No. 4, April 1974, pp. 571-572.

2. Carlson, L.A.: Transonic Airfoil Flowfield Analysis Using Cartesian Coordinates. NASA CR-2577, August 1975.

3. Carlson, L.A.: Transonic Airfoil Design Using Cartesian Coordinates. NASA CR-2578, April 1976.

4. Carlson, L.A.: Transonic Airfoil Analysis and Design Using Cartesian Coordinates. Journal of Aircraft, Vol. 13, No. 5, May 1976, pp. 349-356.

5. Carlson, L.A.: TRANDES: A Fortran Program for Transonic Airfoil Analysis or Design. NASA CR-2821, June 1977.

6. Nash, J.F.; and Macdonald, A.G.J.: The Calculation of Momentum Thickness in a Turbulent Boundary Layer at Mach Numbers up to Unity. Aero. Res. Council, C.P. No. 963, 1967.

7. Carlson, L.A.: Inverse Transonic Airfoil Design Including Viscous Interaction. NASA CP-2001, November 1976, pp. 1387-1395.

8. Jameson, A.: Transonic Flow Calculations for Airfoils and Bodies of Revolution. Grumman Aero. Report 390-71-1, December 1971.

9. Bauer, F.; Garabedian, P.; Korn, D.; and Jameson, A.: Supercritical Wing Sections II. Springer-Verlag, New York, 1975.

10. Freuler, R.J.; and Gregorek, G.M.: An Evaluation of Four Single Element Airfoil Analytic Methods. Advanced Technology Airfoil Research, Volume I, NASA CP-2045, Pt. 1, 1979. (Paper 9 of this compilation.)

11. Stratford, B.S.: The Prediction of Separation of the Turbulent Boundary Layer. Journal of Fluid Mechanics, Vol. 5, Part 1, January 1959, pp. 1-16.

12. Whitcomb, R.T.: Review of NASA Supercritical Airfoils. Proc. of the IXth ICAS Congress, Haifa, Israel, Paper 74-10, August 1974.

13. Barnwell, R.W.: Two Inviscid Computational Simulations of Separated Flow about Airfoils. AIAA Paper 76-379, July 1976.

14. Gross, L.W.: The Prediction of Two-Dimensional Airfoil Stall Progression. AIAA Paper 78-155, January 1978.

15. Henderson, M.L.: A Solution to the 2-D Separated Wake Modeling Problem and its Use to Predict $C_{L_{max}}$ of Arbitrary Airfoil Sections. AIAA Paper 78-156, January 1978.

16. Maskew, B.; and Dvorak, F.A.: Investigation of Separation Models for the Prediction of $C_{L_{max}}$. American Helicopter Society Paper 77-33-01, May 1977.

17. Zumwalt, G.W.; and Nark, S.N.: An Analytical Model for Highly Separated Flow on Airfoils at Low Speeds. Wichita State Univ. Report AR-77-2, May 1977.

18. McGhee, R.J.; Beasley, W.D.; and Somers, D.M.: Low-Speed Aerodynamic Characteristics of a 13-Percent Thick Airfoil Section Designed for General Aviation Applications. NASA TMX-72697, May 1977.

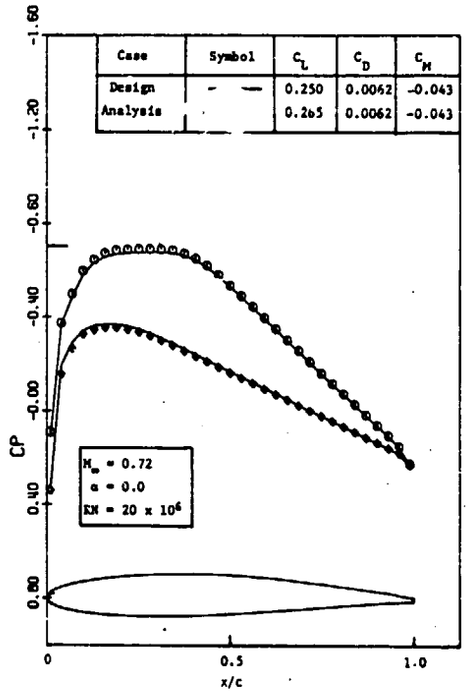

Figure 1.- Airfoil shape and comparison of design and analysis results for a low lift airfoil.

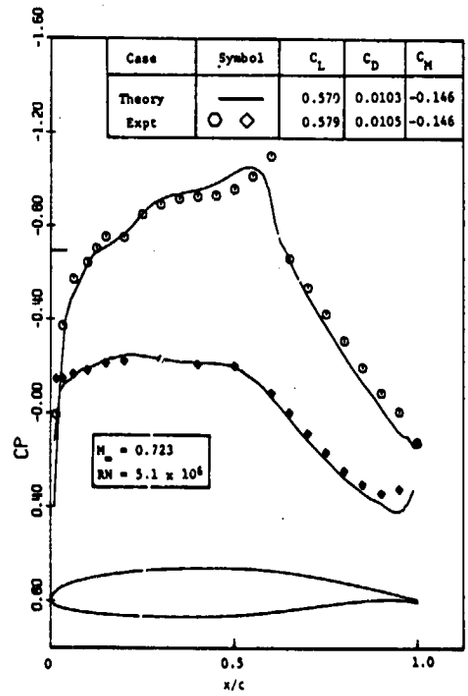

Figure 2.- Comparison of TRANDES analysis results with experimental data for a GA(W)-2 airfoil.

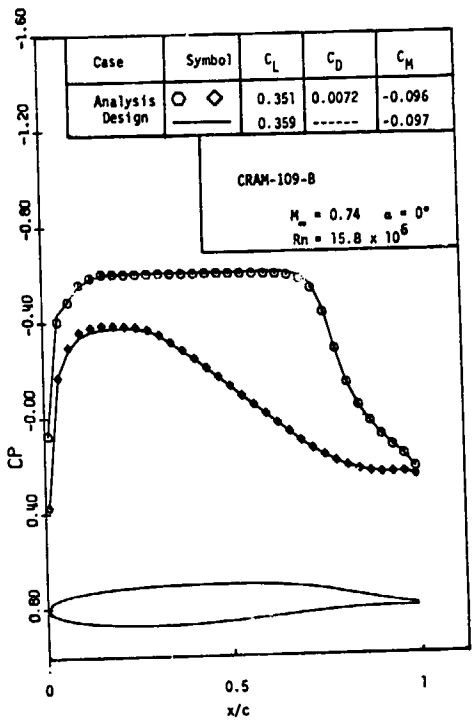

Figure 3.- Profile shape and comparison of design and analysis pressure distributions for CRAM-109-B.

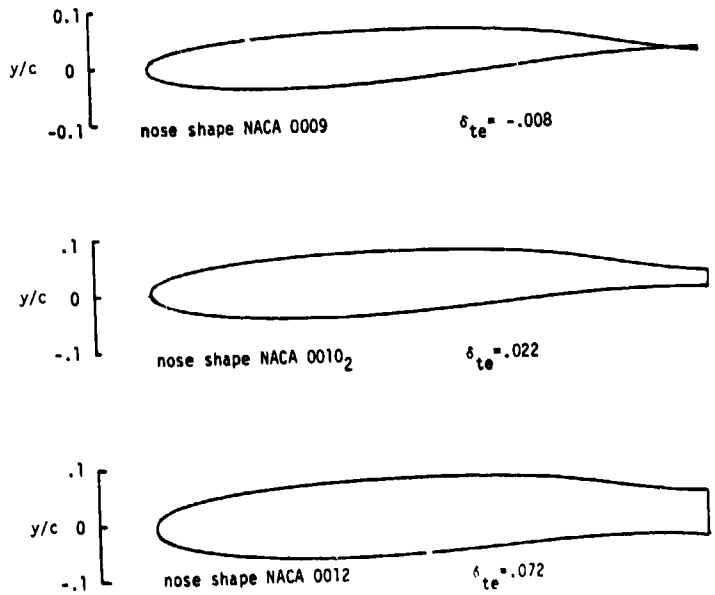

Figure 4.- Variation of trailing-edge thickness with nose-shape thickness for three nose shapes.

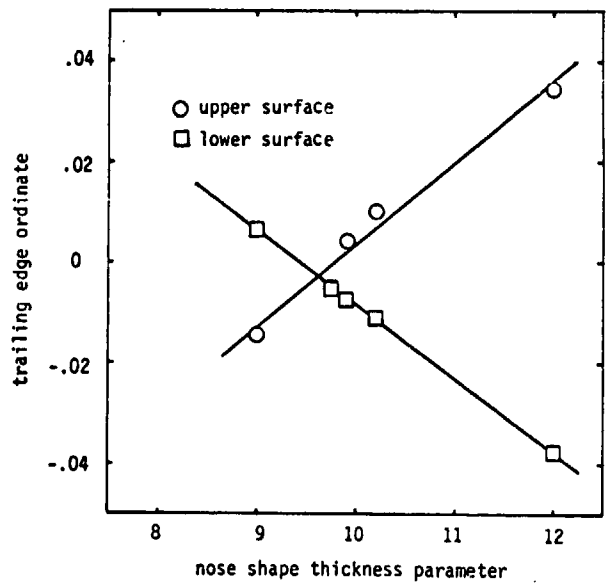

Figure 5.- Variation of trailing-edge ordinates with nose-shape thickness for upper and lower surfaces.

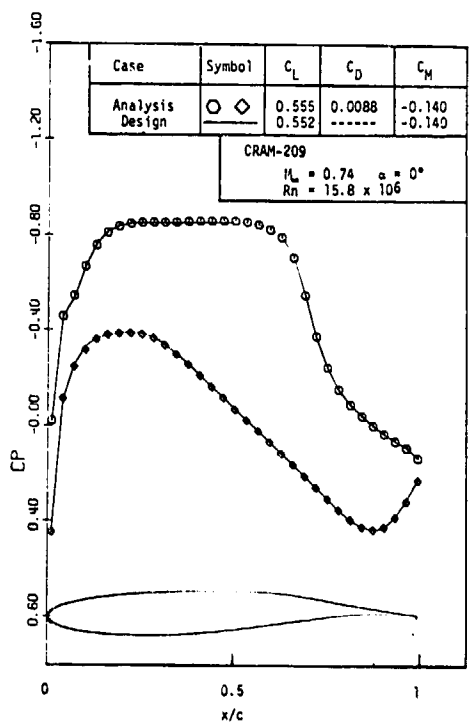

Figure 6.- Profile shape and comparison of design and analysis pressure distributions for CRAM-209.

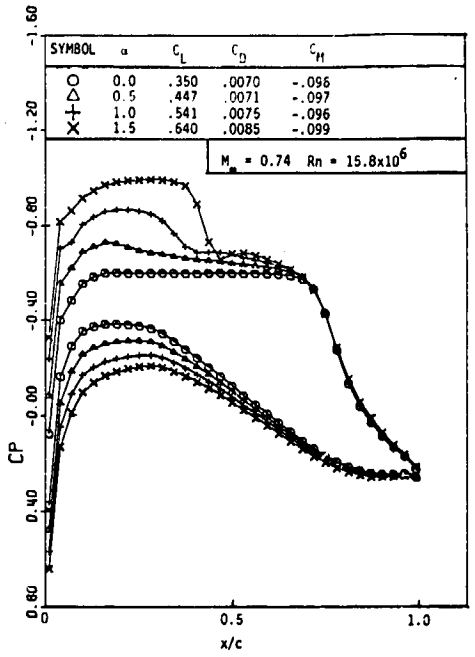

Figure 7.- Comparison of pressure distributions at four angles of attack for CRAM-109-B.

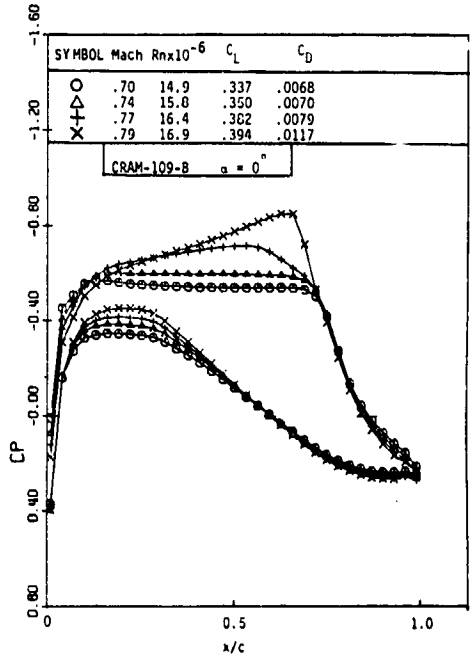

Figure 8.- Comparison of pressure distributions at four Mach numbers for CRAM-109-B.

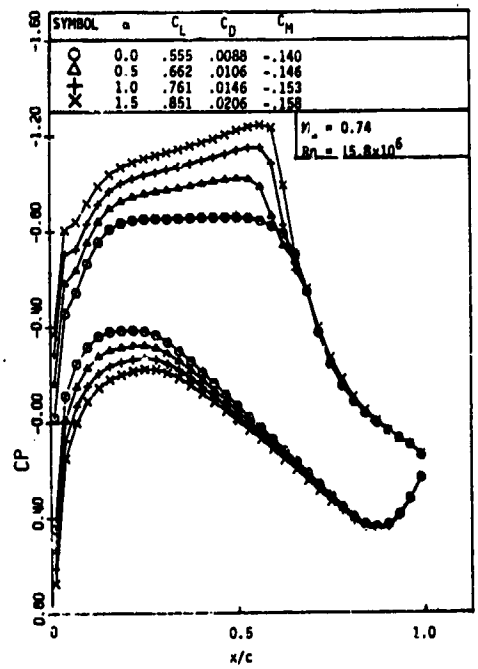

Figure 9.- Comparison of pressure distributions at four angles of attack for CRAM-209.

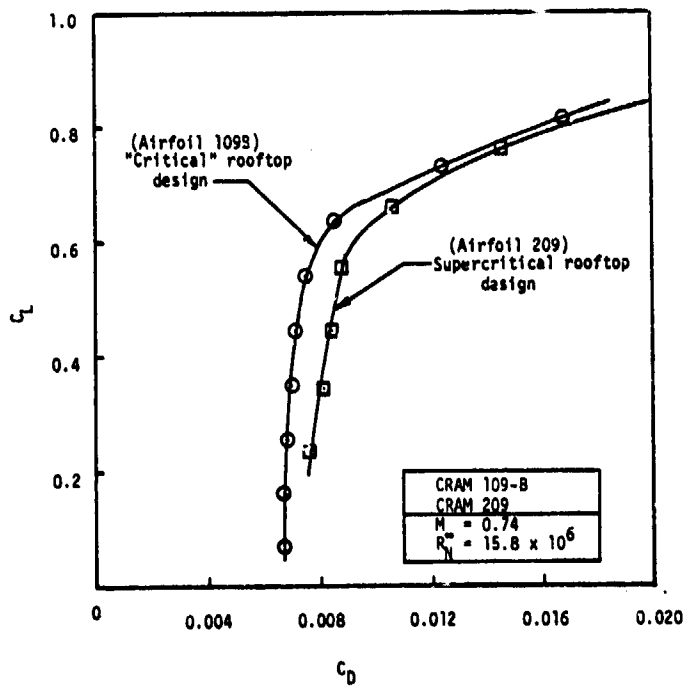

Figure 10.- Comparison of drag polars.

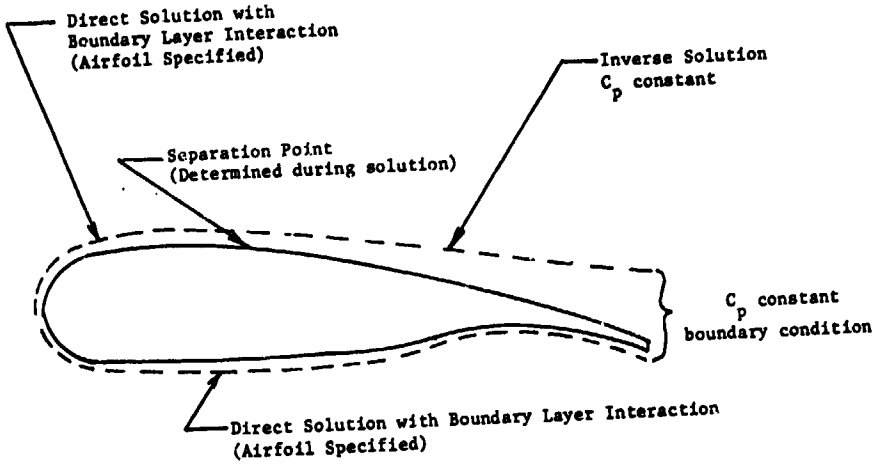

Figure 11.- Problem formulation.

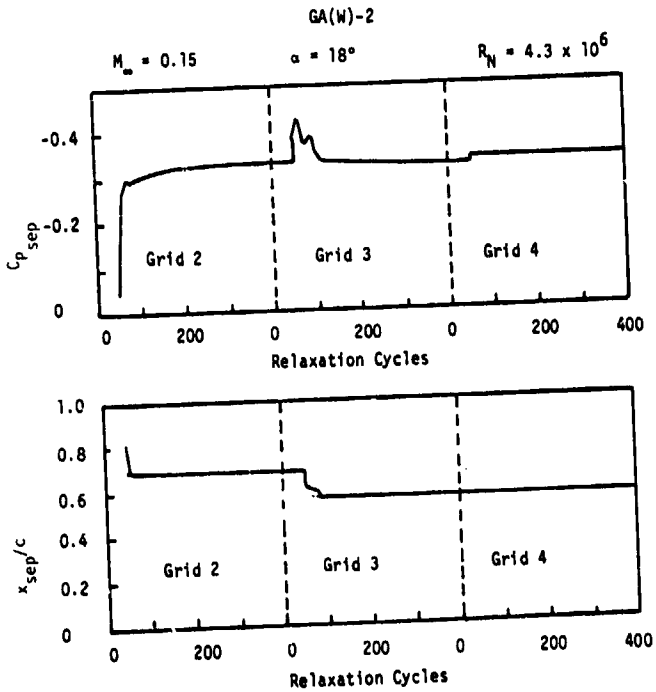

Figure 12.- Separation point and pressure behavior during relaxation process.

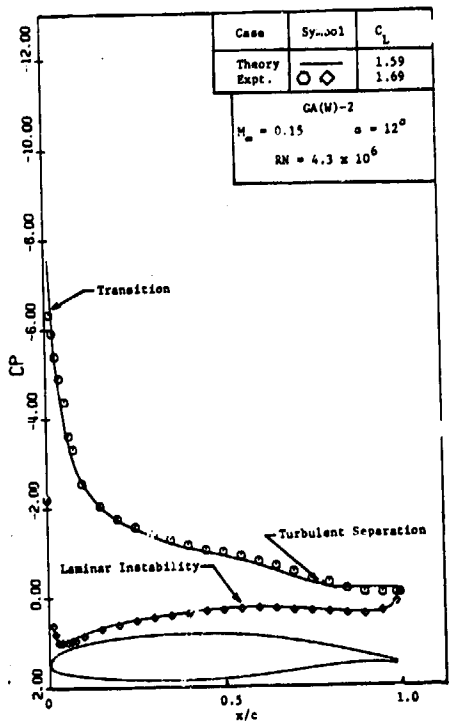

Figure 13.- Theoretical and experimental pressure-distribution comparisons. Laminar turbulent case; $\alpha = 12^{o}$.

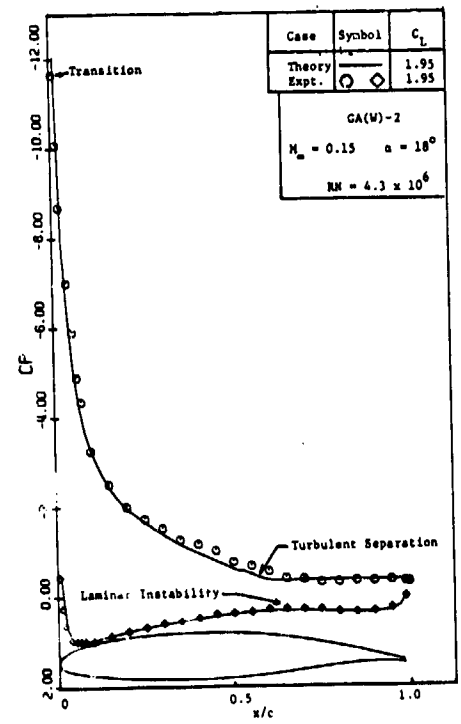

Figure 14.- Theoretical and experimental pressure-distribution comparisons. Laminar turbulent case; $\alpha = 18^{o}$.

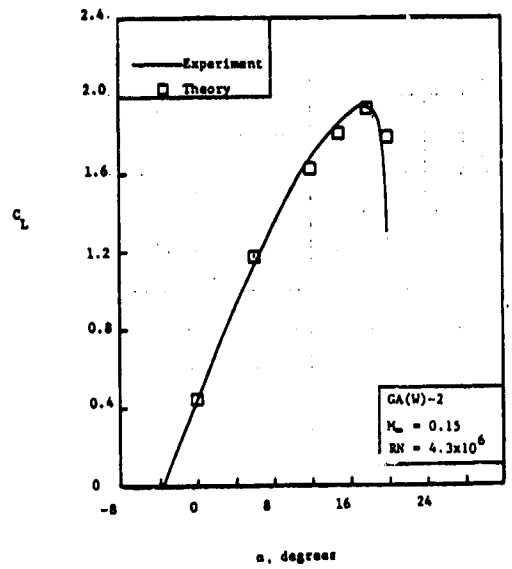

Figure 15.- Comparison of theory and experiment for C_L plotted against α for a GA(W)-2 airfoil.